Received: 11 May 2024 | Revised: 9 July 2024 | Accepted: 18 July 2024 | Published online: 24 July 2024

RESEARCH ARTICLE

Archives of Advanced Engineering Science
2024, Vol. 00(00) 1–7
DOI: 10.47852/bonviewAAES42023402

BON VIEW PUBLISHING

Preparation of Manganese-Doped Bismuth Oxide for the Photocatalytic Degradation of Methylene Blue

Mansoor Jamal[1], Gul Asimullah Khan Nabi[2], Hao Sun[3,4], Khair Ullah[1], Osama Ali Khattak[5], Muhammad Kashif[1,*], Salman Khan[1], Mohsin Alam[1], Shah Hussain[6], Mati Ullah[7], Seeqal Aleena[8], Hameedul Haq[7], Saira Umar[2], Muhammad Atif[9], Ijaz Hussain[9] and Aalia Masood[1]

[1]*Department of Chemistry, Abdul Wali Khan University, Pakistan*

[2]*Department of Chemistry, Bacha Khan University, Pakistan*

[3]*Faculty of Science, Autonomous University of Madrid, Spain*

[4]*Cantoblanco Campus, Consejo Superior de Investigaciones Científicas, Spain*

[5]*College of Chemical Engineering, Taiyuan University of Technology, China*

[6]*Department of Chemistry, Government Postgraduate Collage, Pakistan*

[7]*Department of Physics, Abdul Wali Khan University, Pakistan*

[8]*Institute of Biochemistry and Biotechnology, PMAS Arid Agriculture University, Pakistan*

[9]*Department of Microbiology, Abdul Wali Khan University, Pakistan*

Abstract: The current study describes a unique method for degrading methylene blue dye utilizing Mn-doped Bi_2O_3 nanoparticles (NPs) exposed to UV light. Bi_2O_3 NPs doped with Mn were produced using a hydrothermal process. Scanning electron microscopy (SEM), energy dispersive X-ray analysis (EDX), Fourier transform infrared spectroscopy (FTIR), and X-ray diffraction (XRD) were used to characterize the prepared NPs. It was discovered that the band gaps of Mn/ Bi_2O_3 NPs are 2%, 3%, and 4%, respectively, and are 4.13 eV, 3.92 eV, and 3.77 eV. Functional group identification using FTIR. Mn-doped Bi_2O_3 NPs were captured in SEM pictures at various magnifications, and the photos clearly display the particles' dual morphologies, cubic and cylindrical. The Mn-doped Bi_2O_3 particles were found to be crystalline, with mean diameters of 20 nm, according to the XRD data. The photodegradation efficiency of Mn/Bi_2O_3 at experimental dye concentrations of 2%, 3%, and 4% was determined to be 90.29, 91.6, and 93.16 percent, respectively, over a 150 min time interval. At the ideal catalyst dosage of 0.2 g and concentration of 40 ppm, a high percentage of dye degradation was observed. Numerous metals have been doped into zinc oxides, although no work has documented doping of Bi_2O_3 with Mn. Additionally, it was utilized for the first time to look at the deterioration of methylene blue dye.

Keywords: methylene blue, Mn-doped Bi_2O_3, hydrothermal preparation, double distilled water, photocatalytic degradation

1. Introduction

Humans depend heavily on water, and as a result of urbanization and industrialization, the quality of the water has declined, endangering both humans and other living things. Low water quality has an impact on the economy, agriculture, and food production. Water sources become contaminated with organic dyes and pigments from several sectors, including cosmetics, textile, paper and printing, and soap, making them unsuitable for consumption and other purposes [1]. The quickening rate of development is causing a serious degradation of our freshwater resources. Many poisonous and dangerous materials, including synthetic dyes, which have garnered significant attention, are routinely dumped into the nearby water bodies as a result of insufficient effluent treatment at the source. Through the discharge of industrial effluent into the environment, an estimated 280,000 tones of synthetic dyes are released annually into the planet. Dyes are typically difficult to break down in water due to their composite molecular architectures, which also serve to keep them stable against light and biodegradation. Distillation, leather, paper, textile, fabric, cosmetics, ink, electroplating, food processing, plastic, and pharmaceuticals are among the industries that are the

*Corresponding author: Muhammad Kashif, Department of Chemistry, Abdul Wali Khan University, Pakistan. Email: mkashifsgr1@gmail.com

primary suppliers of dyes. Animal eyes and skin have been adversely impacted by dyes that have persistent colors. Water-containing dyes can lead to developmental, geotaxis, and cancerous illnesses in humans, animals, and microbes. Dyes alter the esthetics of the river by lowering the amount of sunlight that reaches the water, which in turn affects photosynthesis in aquatic greenery. Treatment technology advancements are required to fully break down dyes and organic contaminants found in effluents. Such pollutants can be eliminated using a number of proven techniques, including biological treatment, c-radiolysis, adsorption on activated carbon, ozone/UV/hydrogen peroxide, and hydrogen peroxide/UV radiation. These techniques have several shortcomings in terms of implementation, expense, and efficacy in treating wastewater. However, because they need a lot of time and produce sludge, biological approaches are not feasible [2]. The dyes are colored materials that reduce photosynthetic reactions by obstructing sunlight from entering the water stream. Most dyes are dangerous to people and can cause malignant neoplastic illnesses in animals [3]. Methylene blue (MB) is one commercial dye that poses a serious risk to people, animals, and the environment [4]. Dye has been extracted from wastewater using a variety of processes, including ozonization, chemical coagulation, oxidation, electrolysis, and biodegradation. Nevertheless, the concentration of the pollutants cannot be lowered using these approaches to the appropriate levels [5]. A breakthrough destructive technique known as photocatalysis employing metal oxides has emerged that promises to completely degrade organic contaminants with no negative side effects and at comparatively reduced prices. Both homogeneous and heterogeneous photocatalysts are commonly used in scientific applications. In a homogeneous catalytic reaction system, the catalysts are present as solutes since a catalyst is considered homogeneous if it is present in the same phase as the reagents. If a photocatalyst is present in a phase distinct from the reaction mixture, on the other hand, it can be heterogeneous. The non-toxicity, low cost, ease of separation from the reaction mixture, and reusability are the benefits of heterogeneous catalysts. Good photoactivity, biological and chemical inertness, suitability for absorbing visible or near-UV light, and stability against photocorrosion are all necessary for a perfect photocatalyst. In recent times, the most efficient and cost-effective method for totally destroying dye pollutants has been shown to be photocatalytic degradation when exposed to UV-visible light. By reducing the dyes, this method separates the photocatalyst and produces fewer hazardous byproducts that are easily recyclable. When complex organic pollutants are broken down into harmless carbon dioxide and water, metal oxide nanoparticles (NPs) are the most often used semiconductor photocatalysts for dye degradation [6]. A developing method called the "advanced oxidation process" uses the production of $HO^{\bullet}$, which have a strong corrosion capacity ($E_0 = 2.76$ V) and may completely mineralize organic contaminants. There is no longer a need for secondary disposal using these techniques, which include Fenton ($Fe_2^+ + H_2O_2$), photolysis (UV + H_2O_2), electrolysis (electrodes + current), photo-Fenton (solar light + Fenton), ozone (O_3), sonolysis (ultrasounds), and photocatalysis (light + catalyst) [7–9]. Photocatalysis is defined as the following three processes: absorbing photons with energy higher than a photo catalyst's band gap; migrating, recombining electron-hole pairs, forming, or separating, and lastly, redox reactions at the photo catalyst's surface [10]. Conducting metals (such ZnO, Fe_2O_3, CdS, and Mn-doped Bi_2O_3) can function as sensitizers for light-induced redox reactions because of their crowded valence band and unfilled conduction band [11]. Sulfidation of metals has been shown to improve selectivity and reactivity for organic contaminants while decreasing interactions with water when compared to metal oxides. The primary advantage of metal sulfidation is said to be a combination of improved electron transport and hydrophobicity; this was recently verified by electrochemical testing and measurements of the water contact angle [12]. It is uncertain whether the reactive sites are S or metal sites and how sulfur influences the charge density distribution of metal at the atomistic level because these characterizations are bulk analyses. However, the hydrogen evolution reaction in water is provided by metal sulfide [13]. This is the mechanism by which materials donate electrons to the water, resulting in atomic H (Volmer reaction), which is then mixed to generate H_2 (Heyrovsky reaction or Tafel) on a metal exterior. Despite previous research indicating that contaminants may be broken down by atomic H, H_2, and direct electron transfer [14]. Mn-doped Bi_2O_3 2.42 eV tiny band gap makes it suitable for use in photoluminescent, electroluminescent, and photoconductive devices [15]. Recently, Mn-doped Bi_2O_3 has drawn significant interest due to its remarkable physicochemical features, which include excellent permeability, magnetic properties, distinctive electrical, large specific surface area, and optical [16]. A study was planned to produce and characterize Mn-doped Bi_2O_3 NPs, taking into account the risks connected with dyes in aqueous systems and the significance of these NPs. The current study also sought to determine the impacts of light damage.

This research describes the synthesis of Mn/Bi_2O_3 NPs using a hydrothermal technique, which resulted in a homogeneous shape and good structural stability. The generated materials were examined using standard analytical techniques such as UV-visible, EDX, scanning electron microscopy (SEM), XRD, and FTIR spectroscopy. The degradation of the MB dye under UV light was used to investigate photocatalytic degradation of the synthesized material for the first time as shown in Figure 1 [17].

2. Experimental Work

2.1. Chemicals and reagents

All of the ingredients utilized in the production of Mn/Bi_2O_3 NPs were analytical grades. These include the following: manganese chloride, bismuth nitrate, and citric acid, all of which were utilized without additional treatment after being bought from Sigma Aldrich. Merck Chemical Company supplied reagent-grade MB and sodium hydroxide, which were employed accordingly. Each and every solution was made using double distilled water.

2.2. Instrumentation

UV-visible spectrophotometers (Model Shimadzu UV-1800) from the Advance Research Lab Department of Chemistry at Bacha Khan University Charsadda and a Perkin Elmer FTIR spectrometer version 10.4.00 were used to analyze and characterize the synthesized compounds. The crystalline grain size, phase type, and crystalline structure were all determined using XRD (Model JEOL-300). To determine the material's elemental makeup, EDX (Model Inea 200, UK, firm Oxford) was employed. High-resolution surface morphology of the materials was examined using a SEM (Model No. JEOL-jsm-5910).

2.3. Preparation of Mn-doped bismuth oxide NP

Hydrothermal preparation of Mn/Bi_2O_3 NPs was carried out. First, a mixture was made by dissolving 0.97 grams of bismuth nitrate at a concentration of 1 m in 10 mL of nitric acid. Then, 0.13 grams of citric acid were added to the mixture, and three

Figure 1
Graphical abstract of Mn-doped Bi_2O_3 nanoparticles

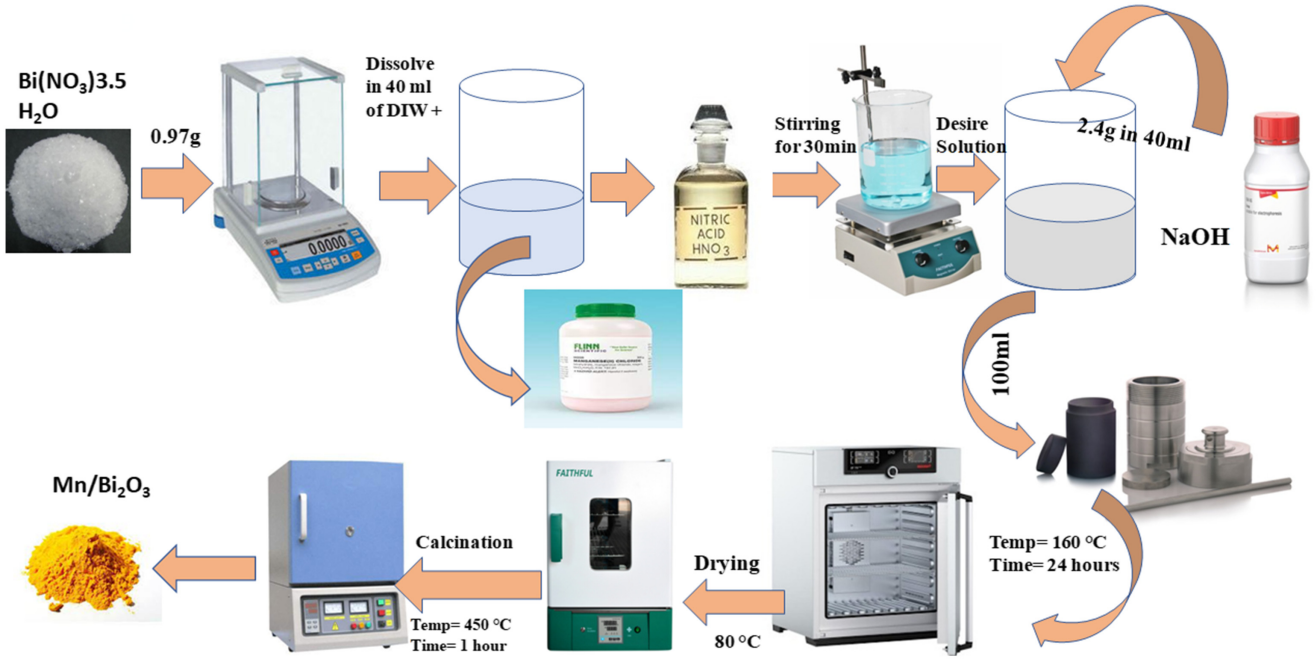

different solutions of bismuth oxide were combined with a manganese chloride solution. After agitating the mixture for fifteen minutes, 2 M sodium hydroxide was progressively added. The mixture was then continuously stirred until the basic pH of the solution was obtained. After obtaining a white precipitate, it was dissolved to create a homogeneous, uniform solution. The solution was heated to 160°C in an oven, and then, it was placed inside an autoclave for 24 h to produce precipitation under high pressure and temperature conditions. The cooled precipitate was centrifuged and cleaned with deionized water and ethanol to eliminate any unreacted reactants. The resultant precipitate was then heated to 160°C for 24 h, and then it was calcined for an hour at 450°C.

2.4. Photocatalytic degradation of MB

The photocatalytic properties of Mn/Bi_2O_3 NPs for the degradation of MB dye were investigated under UV-visible light. To achieve a steady state for adsorption and desorption, 0.2 g of Mn/Bi_2O_3 NPs was added to 100 mL (40 ppm) of dye solution and agitated in the dark for 30 min. Subsequently, the reaction mixture was exposed to UV radiation for 0, 30, 60, 90, 120, and 150 min. Following the reaction, the Mn/Bi_2O_3 NPs were spun out of the mixture, and the UV-visible spectrum was used to determine the dye concentration. The magnitude of the MB absorption peak (664 nm) was measured after some time had passed [18]. This is how the percentage of dye degradation was examined:

$$\text{Degradation efficiency } (\%) = \frac{C_o - C}{C_o} \times 100 \quad (1)$$

where *Co* and *C* stand for the absorbance of the solution, respectively, before and after illuminations.

3. Result and Discussion

3.1. UV-visible spectroscopy

To find the Mn/Bi_2O_3 NPs' maximum absorbance, UV-Vis spectroscopy was used. The wavelength that was used was between 200 and 800 nm. According to Figure 1, the greatest absorbance of Mn/Bi_2O_3 NPs at 2%, 3%, and 4% was seen at 290 nm, 310 nm, and 320 nm. The Tauc figure from Equation (2) was used to calculate the band gap.

$$(\alpha \text{hv})^{1/2} = \beta(\text{hv} - \text{Eg}) \quad (2)$$

where "*n*" is the transition's value; for direct authorized, indirect allowed, direct prohibited, and indirect forbidden transitions, respectively, it can have values of 1/2, 2, 3/2, and 3, where "*Eg*" denotes the band gap, "*hv*" denotes photon energy, and "α" represents the absorption coefficient. Microparticles of Mn/Bi_2O_3 exhibit through acceptable transitions [19]. To determine the band gap, plot $(\alpha h\upsilon)^2$ vs $h\upsilon$ was used to make a graph. After that, the straight line that resulted was extended to the zero absorption coefficients and crossed the x-axis. Mn/Bi_2O_3 NPs had a band gap value of 2%, 3%, and 4%, respectively, of 3.77 eV, 3.92 eV, and 4.13 eV (Figure 2).

3.2. Fourier transform infrared spectrometer (FTIR)

The functional groups of any precursors or additional contaminants were examined, and the purity was verified using FTIR spectroscopy. The 500–4000 cm^{-1} range was covered by the FTIR spectra. The metal-Mn-doped Bi_2O_3 bond is shown by the peak in Figure 2 at 400–700 cm^{-1}. The creation of Mn/Bi_2O_3 NPs is revealed by the range of 730.33 cm^{-1}, which corresponds near the Bi-O & Mn-O bonding mode. The presence of O-H

Figure 2
UV-visible spectra of Mn-doped Bi_2O_3 NPs

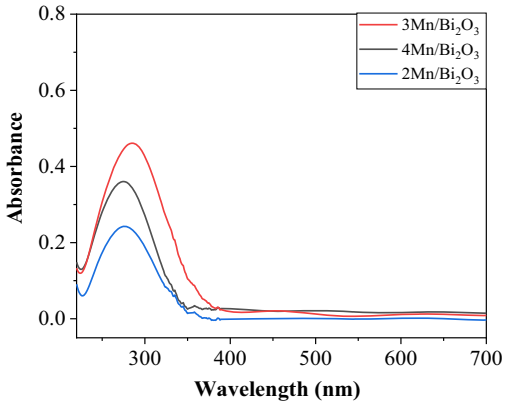

(hydroxyl group) due to moisture absorption by Mn/Bi_2O_3 NPs is accredited to the broad peak detected at 3500–3000 cm^{-1}. Organic impurities were suspected due to the symmetric C≡C bond mode observed at 1500–600 cm^{-1}, resulting from the asymmetric stretching of the C=C bond. The C-O stretching vibration is the cause of the infrared bands as shown in Figure 3 between 3000 cm^{-1} and 3280 cm^{-1}.

3.3. X-ray diffraction analysis (XRD)

A grind XRD study was performed to examine the phase, size, and crystallinity of the NPs. The absence of an additional peak signifies the synthesized NPs' purity [20]. (Figure 4) XRD pattern of Mn/Bi_2O_3 NPs revealed a monochromatic pattern. The diffraction peaks at 2θ were identified as characteristic (111), (220), (311), (400), (511), and 66.7 for Mn/Bi_2O_3 NPs. The peaks were seen at 20.85, 31.15, 37.7, 44.6, 60.3, and 66.7. Using the Debye Scherrer equation, the average crystalline structure for Mn/Bi_2O_3 was determined to be 20 nm, respectively.

$$D = \frac{K\lambda}{\beta D cos\theta} \quad (3)$$

where λ is the X-ray radiation wavelength (1.542 A), βD is the peak width at half maximum intensity, θ is the peak position, and D is the crystallite size of NPs in nm [21, 22].

Figure 3
FTIR spectrum of Mn-doped Bi_2O_3 NPs

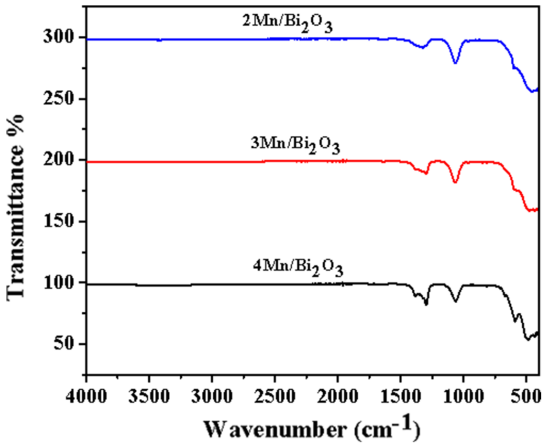

Figure 4
XRD Mn-doped Bi_2O_3 NPs

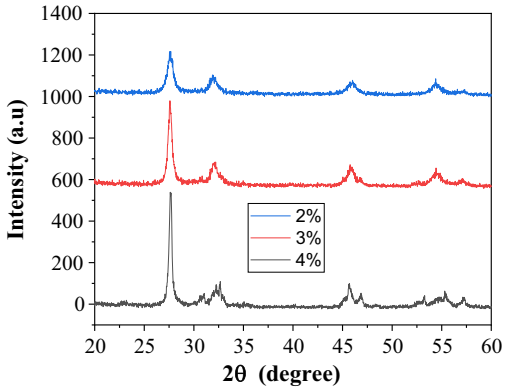

3.4. EDX analysis

The EDX spectra confirm the diffusion of the Mn/Bi_2O_3 NPs lattice and demonstrate the exceptional purity of the synthesized Mn/Bi_2O_3 nanomaterials, which are free of any external contaminants. Figure 5 displays the detected atomic percentages for all the elements that were too close to the target material. The weight percentages of C, O, and Bi in Mn/Bi_2O_3 were 25.14%, 21.68%, and 53.18%, respectively.

3.5. SEM

The distribution of the dopant (manganese) throughout the bismuth oxide matrix is investigated using SEM. This can involve figuring out if the dopant is evenly distributed or if it gathers in the substance to form aggregates or clusters. SEM and EDX spectroscopy can reveal information on the constituent elements of a substance. This makes it possible to calculate the relative concentrations of bismuth oxide and manganese in the sample, together with any additional pollutants or impurities that could be present. SEM pictures of Mn/Bi_2O_3 NPs acquired at different magnifications are seen in Figure 6a, b, c, d. The SEM picture makes it evident that the surfaces of the NPs with lower Mn dopant concentrations are smooth. Particles with rounded and cylindrical shapes are ostensibly found in a variety.

3.6. Photocatalytic activity

The removal of MB dye under UV light illumination was used to assess the photocatalytic commotion of Mn/Bi_2O_3 nanomaterials. Round-bottom photocatalytic cells were used to conduct the photocatalytic processes. The solution was originally kept in the dark to achieve adsorption-desorption equilibrium [23]. Using a UV-visible spectrophotometer, samples were taken and examined at each time point in the experimental data. The dye's lambda max was measured at 664 nm, and this wavelength served as a reference for further research. Using Equation (4), the % deterioration was determined.

$$\%\,(\text{Degradation}) = \frac{A_o - A}{A_o} \times 100 \quad (4)$$

where A_o shows the initial dye concentration, while A shows the dye concentration after the UV irradiation.

Figure 7 illustrates the variations in the percent degradation of MB dye with a concentration of 40 ppm exposed to UV light over a

Figure 5
EDX Mn-doped Bi_2O_3 NPs

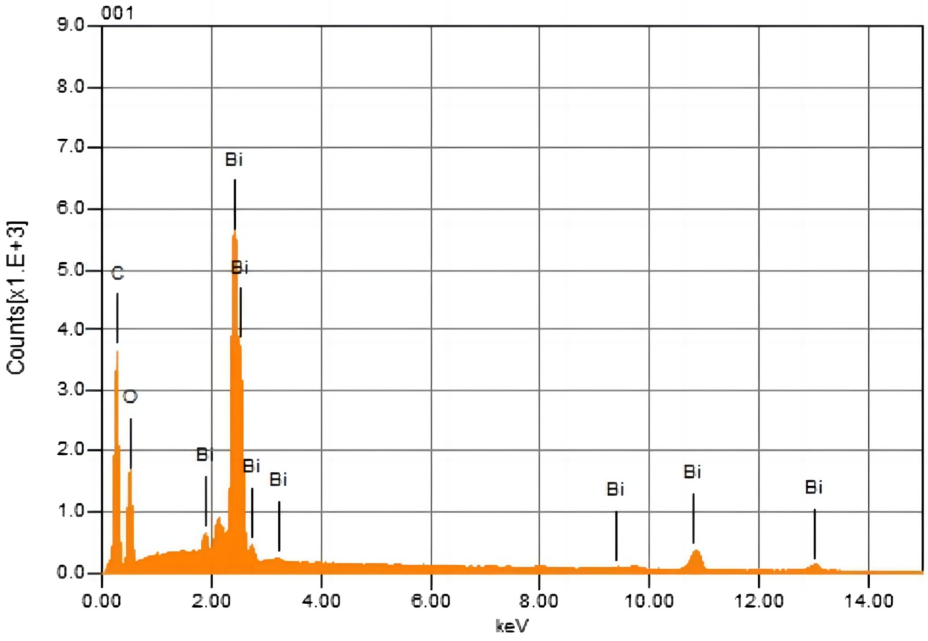

Formula	mass%	Atom%	Sigma	Net	K ratio	Line
C	25.14	56.52	0.02	92543	0.0249772	K
O	21.68	36.60	0.08	41894	0.0516712	K
Bi	53.18	6.87	0.17	398220	0.3092040	M
Total	100.00	100.00				

Figure 6
SEM images Mn-doped Bi_2O_3 NPs

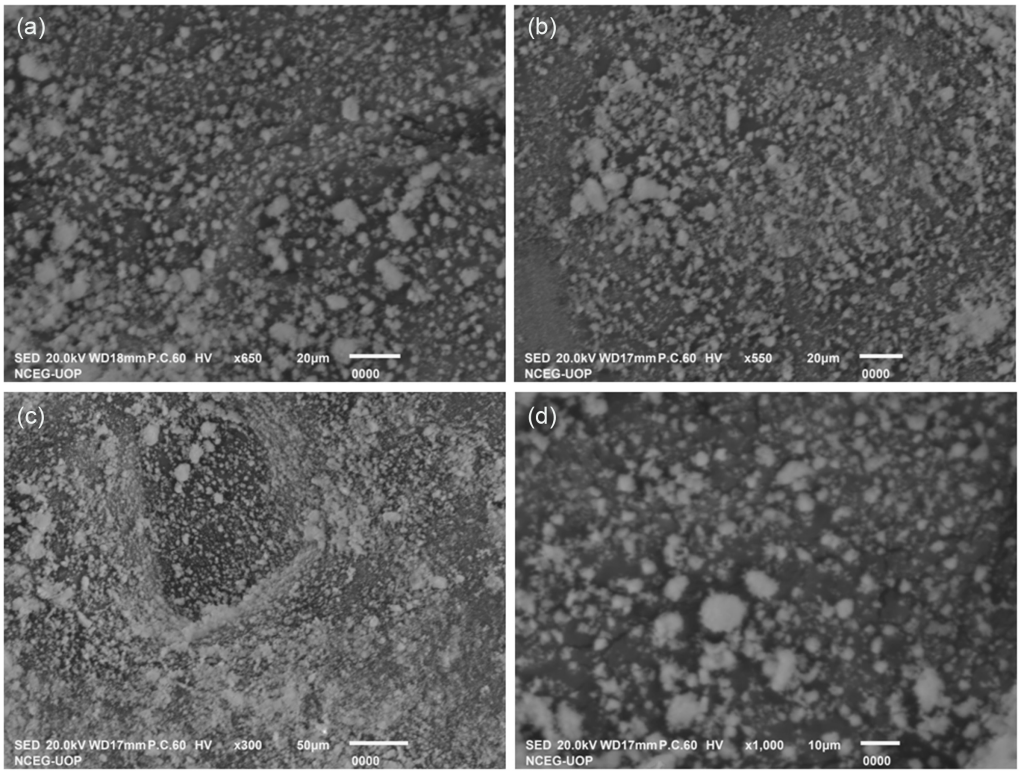

Figure 7
UV-visible spectra (a) 2Mn/Bi_2O_3, (b) 3Mn/Bi_2O_3, (c) 4Mn/Bi_2O_3, and (d) photocatalytic degradation of methylene blue using 2, 3, 4 Mn/Bi_2O_3 nanoparticles

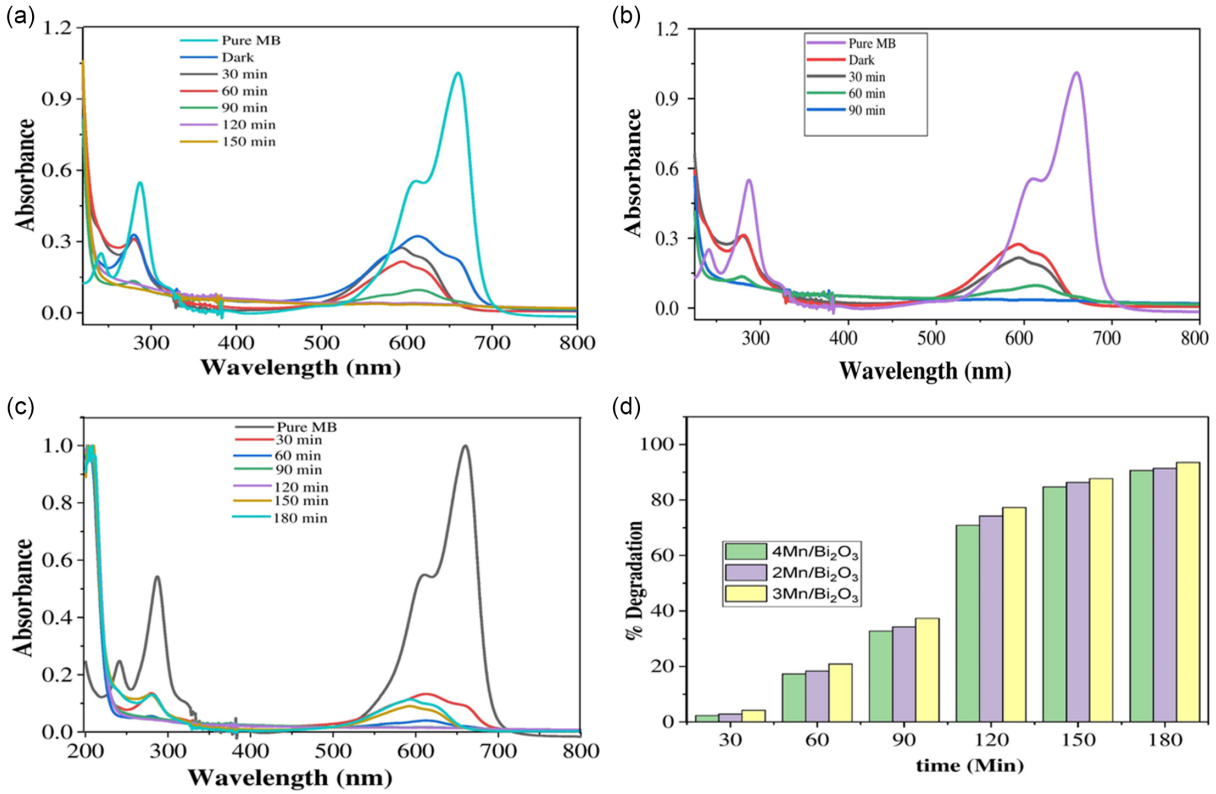

Table 1
Photocatalytic removal of MB dye on dissimilar ratios of 2, 3, 4 Mn/Bi_2O_3 NPs

	% (Degradation)		
Time (min)	2Mn/Bi_2O_3	3Mn/Bi_2O_3	4Mn/Bi_2O_3
0	2.01	3.73	2.29
30	14.85	26.98	17.31
60	37.89	77.52	32.79
90	72.02	90.83	70.87
120	87.95	93.16	84.72
150	90.29	———	91.64

30-minute period using 0.2 g/100mL of photocatalysts (2Mn/Bi_2O_3, 3Mn/Bi_2O_3, and 4Mn/Bi_2O_3). The graphs show that as the irradiation period increases, the dye's % degradation utilizing the catalysts (2Mn/Bi_2O_3, 3Mn/Bi_2O_3, and 4Mn/Bi_2O_3) increases. At every experimental dye concentration, the photodegradation efficiency of 2Mn/Bi_2O_3, 3Mn/Bi_2O_3, and 4Mn/Bi_2O_3 was determined to be 90.29, 93.16, and 91.64%, respectively, following a 150 min time interval. The interaction between photons and the photocatalyst is directly impacted by the length of the radiation. Longer radiation times result in the formation of more O-H radicals. A change in the photocatalyst absorption properties also affects the dye's degradation. Table 1 illustrates the significant deterioration of the 2Mn/Bi_2O_3 and 4Mn/ Bi_2O_3 NPs as compared to the 3Mn/ Bi_2O_3.

4. Conclusion

Mn/Bi_2O_3 photocatalyst has been used to photocatalytically degrade the cationic dye MB in the presence of UV light. The band gap of the effectively synthesized Mn/Bi_2O_3 is 4.13 eV, 3.92 eV, and 3.77 eV for the 2%, 3%, and 4% NPs produced via the green approach, respectively. For elemental composition, FTIR spectroscopy and EDX analysis are used to identify functional groups. Mn/Bi_2O_3 NPs were captured in SEM pictures at various magnifications, and the photos clearly display the particles' dual morphologies, cubic and cylindrical. The Mn/Bi_2O_3 particles were found to be crystalline, with mean diameters of 20 nm, according to the XRD data. Using Mn/Bi_2O_3 at 2%, 3%, and 5% NPs, respectively, 150 min of dye degradation was observed, yielding results of approximately 90.29, 91.6, and 93.16 percent.

Ethical Statement

This study does not contain any studies with human or animal subjects performed by any of the authors.

Conflicts of Interest

The authors declare that they have no conflicts of interest to this work.

Data Availability Statement

Data available on request from the corresponding author upon reasonable request.

References

[1] Kashif, M., Muhammad, S., Ali, A., Ali, K., Khan, S., Zahoor, S., & Hamza, M. (2023). Bismuth oxide nanoparticle fabrication and characterization for photocatalytic bromophenol blue degradation. *Journal of Xi'an Shiyou University*, *19*(7), 521–544.

[2] Salama, A., Mohamed, A., Aboamera, N. M., Osman, T. A., & Khattab, A. (2018). Photocatalytic degradation of organic dyes using composite nanofibers under UV irradiation. *Applied Nanoscience*, *8,* 155–161.

[3] Naz, F., & Saeed, K. (2021). Investigation of photocatalytic behavior of undoped ZnO and Cr-doped ZnO nanoparticles for the degradation of dye. *Inorganic and Nano-Metal Chemistry*, *51*(1), 1–11.

[4] Khairnar, S. D., & Shrivastava, V. S. (2019). Facile synthesis of nickel oxide nanoparticles for the degradation of methylene blue and Rhodamine B dye: A comparative study. *Journal of Taibah University for Science*, *13*, 1108–1118.

[5] Arques, A., Amat, A. M., Garcia-Ripoll, A., & Vicente, R. (2007). Detoxification and/or increase of the biodegradability of aqueous solutions of dimethoate by means of solar photocatalysis. *Journal of Hazardous Materials*, *146*, 447452.

[6] Khan, A., Valicsek, Z., & Horváth, O. (2020). Synthesis, characterization and application of iron (II) doped copper ferrites ($CuII(x)\ FeII(1-x)\ FeIII_2O_4$) as novel heterogeneous photo-Fenton catalysts. *Nanomaterials*, *10*, 921.

[7] Sharfalddin, A., Alzahrani, E., & Alamoudi, M. (2016). Micro, sono, photocatalytic degradation of eosin B using ferric oxide doped with cobalt. *American Chemical Science Journal*, *13*(3), 1–13.

[8] Kaur, J., Sharma, M., & Pandey, O. P. (2014). Synthesis, characterization, photocatalytic and reusability studies of capped ZnS nanoparticles. *Bulletin of Materials Science*, *37*, 931–940.

[9] Hasani, K., Peyghami, A., Moharrami, A., Vosoughi, M., & Dargahi, A. (2020). The efficacy of sono-electro-Fenton process for removal of Cefxime antibiotic from aqueous solutions by response surface methodology (RSM) and evaluation of toxicity of effluent by microorganisms. *Arabian Journal of Chemistry*, *13*, 6122–6139.

[10] Sirés, I., Brillas, E., Oturan, M. A., Rodrigo, M. A., & Panizza, M. (2014). Electrochemical advanced oxidation processes: Today and tomorrow: A review. *Environmental Science and Pollution Research*, *21*, 8336–8367.

[11] Aponte, Á. G., Ramírez, M. A. L., Mora, Y. C., Santa Marín, J. F., & Sierra, R. B. (2020). Cerium oxide nanoparticles for color removal of indigo carmine and methylene blue solutions. *AIMS Materials Science*, *7*, 468–485.

[12] Singh, A., Goyal, V., Singh, J., & Rawat, M. (2020). Structural, morphological, optical and photocatalytic properties of green synthesized TiO_2 NPs. *Current Research in Green and Sustainable Chemistry*, *3*, 100033.

[13] Xu, J., Avellan, A., Li, H., Liu, X., Noël, V., Lou, Z., & Lowry, G. V. (2020). Sulfur loading and speciation control the hydrophobicity, electron transfer, reactivity, and selectivity of sulfidized nanoscale zerovalent iron. *Advanced Materials*, *32*(17), 1906910.

[14] Li, H., Yang, W., Wu, C., & Xu, J. (2021). Origin of the hydrophobicity of sulfur-containing iron surfaces. *Physical Chemistry Chemical Physics*, *23*, 13971–13976.

[15] Cao, Z., Li, H., Lowry, G. V., Shi, X., Pan, X., Xu, X., & Xu, J. (2021). Unveiling the role of sulfur in rapid defluorination of florfenicol by sulfidized nanoscale zero-valent iron in water under ambient conditions. *Environmental Science & Technology*, *55*(4), 26282638.

[16] Venkatesh, N., Sabarish, K., Murugadoss, G., Thangamuthu, R., & Sakthivel, P. (2020). Visible light-driven photocatalytic dye degradation under natural sunlight using Sn-doped CdS nanoparticles. *Environmental Science and Pollution Research*, *27*, 43212–43222.

[17] Rafati, A. A., Borujeni, A. R. A., Najaf, M., & Bagheri, A. (2011). Ultrasonic/surfactant assisted of CdS nano hollow sphere synthesis and characterization. *Materials Characterization*, *62*, 94–98.

[18] Mansoor, S., Nabi, G. A. K., Hussain, S., Javid, Z., & Jan, F. A. (2023). Synthesis, characterization, kinetic and thermodynamic study of photocatalytic degradation of malachite green dye using MnO_2 nanoparticles as catalyst. *Chemistry Africa*, *7*(3), 1575–1583.

[19] Naz, F., Nabi, G. A. K., Nawaz, A., Ali, S., & Siddique, M. (2022). A novel approach for the photocatalytic degradation of binary dyes mixture using SnO_2 nanoparticles as a catalyst. *Journal of Cluster Science*, *34*(4), 2047–2066.

[20] Rashidi, L. (2021). Magnetic nanoparticles: Synthesis and characterization. In A. Ehrmann, T. A. Nguyen, M. Ahmadi, A. Farmani & P. Nguyen-Tri (Eds.), *Magnetic nanoparticle-based hybrid materials*. Woodhead Publishing.

[21] Chattopadhyay, S., Dash, S. S., Kar Mahapatra, S., Tripathy, S., Ghosh, T., Das, B., . . . , & Roy, S. (2014). Chitosan-modified cobalt oxide nanoparticles stimulate TNF-α-mediated apoptosis in human leukemic cells. *JBIC Journal of Biological Inorganic Chemistry*, *19*, 399–414.

[22] Besbes, S., Blecker, C., Deroanne, C., Llognay, G., Drira, N., & Attia, H. (2004). Quality characteristics and oxidative stability of date seed oil during storage. *Food Science and Technology International*, *10*, 333–338.

[23] Haider, F., Nabi, G. A. K., Shah, K., Khan, K. A., & Khan, H. (2023). Green synthesis and electrochemical study of undoped and doped Al_2O_3 nanoparticles using hibiscus rosa-sinensis leaves extract. *Indonesian Journal of Chemistry*, *23*(4), 913–923

How to Cite: Jamal, M., Khan Nabi, G. A., Sun, H., Ullah, K., Khattak, O. A., Kashif, M., Khan, S., Alam, M., Hussain, S., Ullah, M., Aleena, S., Haq, H., Umar, S., Atif, M., Hussain, I., & Masood, A. (2024). Preparation of Manganese-Doped Bismuth Oxide for the Photocatalytic Degradation of Methylene Blue. *Archives of Advanced Engineering Science*. https://doi.org/10.47852/bonviewAAES42023402